Int. J. Heat Mass Transfer. Vol. 34, No. 9, pp. 2291–2301, 1991
Printed in Great Britain

0017–9310/91 $3.00 + 0.00

A heat flux-meter for ash deposit monitoring systems—I. Ash deposit prevention

BRANISLAV BRAJUSKOVIC, MIODRAG MATOVIC† and NAIM AFGAN
Boris Kidric Institute of Nuclear Sciences, 11 001 Belgrade, Yugoslavia

(*Received* 18 *December* 1989 *and in final form* 26 *October* 1990)

Abstract—An air stream cooled 'clean' heat flux-meter has been developed. The results of the experimental and analytical investigation of the cooling air stream curtain that also protects against particle deposit formation are presented. The velocity fields at two different air flow rates and in two perpendicular planes of the stream are mapped using LDA. These data are used to compute ash particle trajectories. Computed ash particle trajectories indicate that the air stream efficiently protects the receiving element of the 'clean' heat flux-meter against ash deposit formation.

INTRODUCTION

THE EXTENSIVE use of low quality coals with a high ash content in modern power plants over the last decade has necessitated heat transfer surface fouling control [1, 2]. The currently used method of ash deposit fouling control in large utility boiler furnaces consists of the use of various types of soot blowers. Operational experience indicates that, apart from the type of blower, efficient and careful deposit control requires the timely scheduling of blower operation. This is particularly the case if water blowers are used where damage to tube walls due to the direct contact of water jets and tube walls at high temperatures has to be minimized.

Blower operation can be properly scheduled only if information on furnace ash deposit formation is available. Due to the complexity of deposit formation processes and heat transfer through ash deposit layers, the extent of these deposits in large utility boiler furnaces can be estimated only through their effect on overall furnace heat transfer. Several different monitoring system types that operate by evaluating the effect of ash deposit on overall furnace heat transfer have been developed [3–5]. Among these, monitoring systems that compare signals from the so-called 'fouled' and 'clean' heat flux-meters yield the most reliable data [3, 4].

In order to ensure ash deposit monitoring system zonal flexibility a new type of 'clean' heat flux-meter has been developed. The design of this heat flux-meter, the experimental mapping of its air stream curtain velocity fields and ash particle trajectory predictions are presented.

DESIGN OF THE 'CLEAN' HEAT FLUX-METER

The new compact and easy to install 'clean' flux-meter reported has an air stream curtain that efficiently cools and protects it against fouling. Our design is based on the easy to install heat flux-meter with a disc type receiving element concept [6, 7]. To maintain compactness and simplicity the air stream both protects against fouling and acts as a heat sink. The developed design is shown in Fig. 1.

Two narrow ribs (3) connect the disc type receiving element (1) to the cylindrical housing (2). Semicircular gaps (4) between the disc and housing serve as air stream outlets and due to their shape the air stream protectively envelops the receiving element. Thermocouples (5) are attached to the receiving disc at its centre and at its perimeter. An insulation layer (6) prevents heat transfer from the back surface of the receiving disc and protects the thermocouple junctions from the air stream. Air is supplied through steel tubes (7). The tubes also act as protective thermocouple leads. To prevent air leakage, a plug (8) is attached to the back of the housing. The 'clean' heat flux-meter is mounted on an actual furnace tube (9).

EXPERIMENTAL EVALUATION OF THE VELOCITY FIELDS

The air stream velocity field was mapped using LDA. Measurements were made in two planes that intersect at right angles at the centre of the receiving disc and are perpendicular to the disc surface. One of the planes passes through the axis of the connecting ribs. Seven velocity profiles were mapped at axial distances of 1, 5, 10, 20, 40, 70 and 100 mm. The measurements are made at two air flow rates, $\dot{V}_1 = 4.6 \times 10^{-3}\ \mathrm{m^3\ s^{-1}}$ and $\dot{V}_2 = 6.8 \times 10^{-3}\ \mathrm{m^3\ s^{-1}}$.

Experimental set-up

A one-component He–Ne 15 mW LDA system was used for the velocity field mapping. A 250 mm focal distance frontal lens and 300 mm focal distance receiving lens placed 27° off axis ensured good spatial resolution. The resulting measuring volume is 0.15 mm

†Present address: Department of Mechanical Engineering, Queen's University, Kingston, Ontario, Canada.

NOMENCLATURE

A_p	ash particle cross-section area
C_D	drag coefficient
d_p	ash particle diameter
F_i	external forces
G	ash particle weight
L	axial distance
m_p	ash particle mass
p	pressure
r	radial coordinate
r_p	ash particle radius
Re_p	ash particle Reynolds number
u	axial component of gas velocity
u_p	axial component of ash particle velocity
v	radial component of gas velocity
v_p	radial component of ash particle velocity
$\dot{V}$	flow rate
V_{FG}	flue gas velocity
V_p	ash particle velocity.

Greek symbols

μ	dynamic viscosity of gas
ρ	gas density
ρ_p	ash particle density
τ	time
τ_p	particle characteristic time
$\Delta\tau$	calculation time interval
ϕ	time constant.

Superscripts

0	value in the previous iteration
$'$	region aside annular gaps
$''$	region above annular gaps.

Subscripts

FG	flue gases
g	gas
p	particle.

in diameter and 0.38 mm long. A fast A/D converter/memory was used for data acquisition. The Doppler bursts were led to and processed by a HP A700 minicomputer using the ACVR code [8, 9].

The measuring system layout is shown in Fig. 2. This modular system consists of the laser (1) and its power supply (2), the transmission optics module (3) with the DUAL Bragg cell driver (4), OEI receiving optics (5) with photo multiplier (6) and power supply (7), an OEI variable band-pass filter (8), an IWATSY DM 901 A/D converter/memory (9) and the HP A700 minicomputer (10).

Commercial grade ZnO powder introduced through a custom made fluidized bed seeder (11) was used to seed the air stream. Due to high outlet velocities and a large jet expansion ratio, a high particle concentration was needed to ensure reasonable data rates, particularly when profiles far from the nozzle are mapped. Due to the high concentration, particle agglomeration could not be avoided completely.

Velocities were measured at 27 points at axial distances of 1–40 mm and at 17 measuring points at axial distances of 70 and 100 mm. A custom made tri-axial traversing stand was used for exact positioning.

Experimental results

Experimental results obtained for air flow rates of 4.6×10^{-3} and 6.8×10^{-3} m^3 s^{-1} are shown in Figs. 3 and 4. The upward vertical flow direction is assumed positive for the u-component of the air flow velocity. For the v-component, left to right is assumed as the positive flow direction. The presented results show

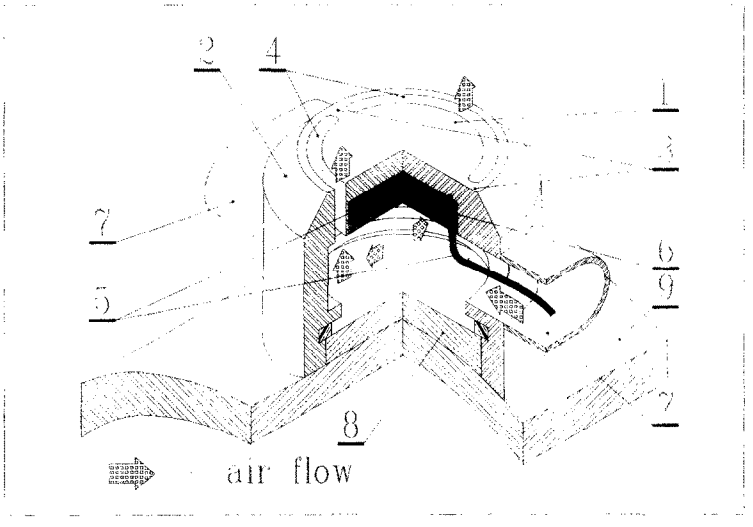

FIG. 1. 'Clean' heat flux-meter.

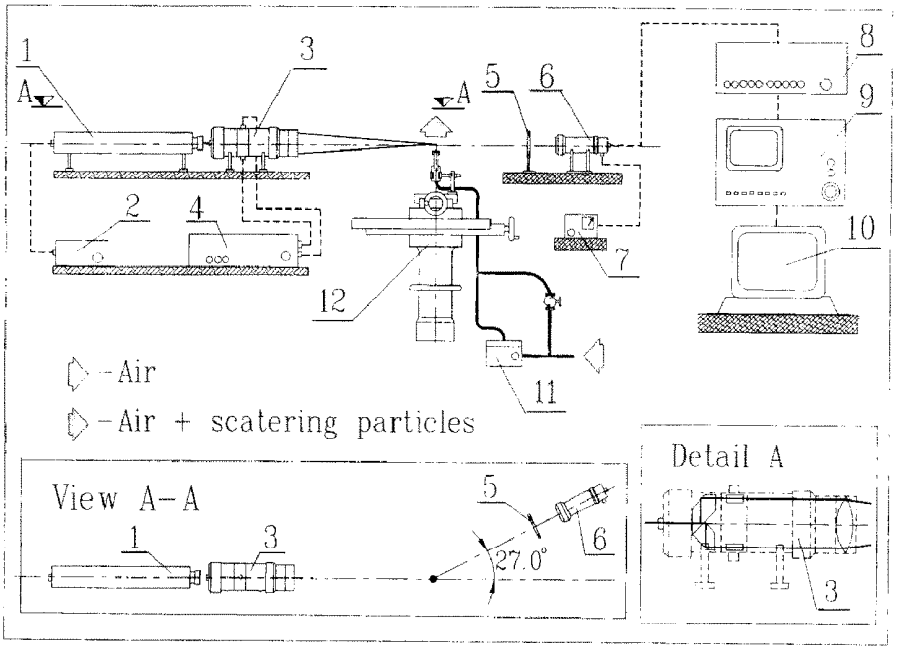

FIG. 2. The LDA system layout.

that the air streams, which are toroidal in the near field, become homogeneous conical shapes in the far field region. At flow rates of 4.6×10^{-3} and 6.8×10^{-3} m^3 s^{-1} the transformation ends at a distance of approximately 40 and 20 mm, respectively. The obtained negative values of the u-component of velocity (Figs. 3 and 4) attest to the existence of a recirculation zone above the receiving disc. The intensity of recirculation is directly proportional to the air flow rate.

The highest values of the u-component of velocity in the plane perpendicular to the connecting ribs were measured in the toroidal stream region, above the gaps (Fig. 3). In the air stream conical region the maximum values of the u-component were measured on the stream axis and are lower than in the toroidal region. The measured values are dependent on the air flow rate and axial distance. At 4.6×10^{-3} m^3 s^{-1} a maximum value of 104 m s^{-1} was measured at an axial distance of 1 mm from the receiving disc. At 6.8×10^{-3} m^3 s^{-1} the maximum value of 139 m s^{-1} was measured at axial distances of 1 and 5 mm from the receiving disc. The maximum negative value of the u-component (-11.0 m s^{-1}) at 6.8×10^{-3} m^3 s^{-1} was also measured at a distance of 1 mm from the receiving disc. At 4.6×10^{-3} m^3 s^{-1} the maximum negative u-component value (-1.1 m s^{-1}) was measured at a distance of 5 mm from the receiving disc. All the negative values of the u-component were measured above the receiving disc.

The highest v-component values in the plane perpendicular to the connecting ribs were measured at an axial distance of 1–5 mm above the receiving disc (Fig. 3). The maximum measured values are 17 and 24 m s^{-1} for 4.6×10^{-3} and 6.8×10^{-3} m^3 s^{-1}, respectively. These values do not exceed 20% of the maximum values of the u-component measured at the same distance and in the same plane.

Results obtained in the plane passing through the connecting ribs indicate their strong effect on the velocity field (Fig. 4). The u-component values measured near the ribs (at an axial distance of 1–10 mm) are considerably lower. The profiles at a distance of 40 mm and greater are similar in shape in both planes. At distances of 1 and 5 mm the maximum v-component values measured in the plane containing the ribs are 30% higher than in the plane perpendicular to the ribs. At greater downstream distances the measured v-component values are alike in both planes.

ASH PARTICLE TRAJECTORIES

The LDA mapped velocity field data are used to numerically predict ash particle trajectories in an attempt to estimate the capability of the air curtain to protect the receiving disc surface against deposit formation.

Gas stream particle movement is influenced by numerous phenomena. According to the literature [10–12], among the most influential are momentum, heat and mass transfer between phases, gas flow turbulence, particle/particle interactions, flow boundary effects, migration of the particles perpendicular to the flow direction and the particle shape. For the present analysis of ash particle movement in an air stream the following effects are neglected:

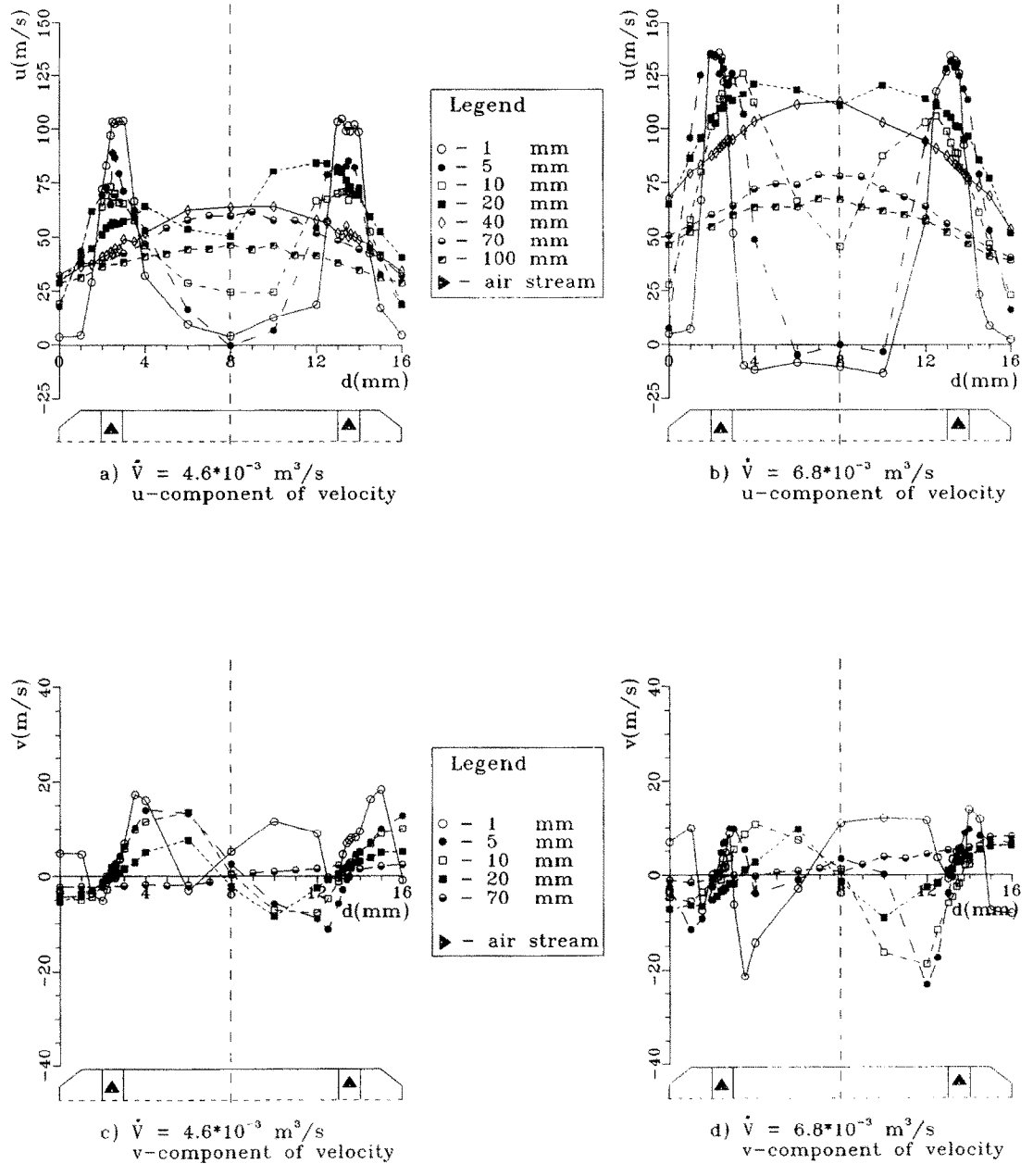

FIG. 3. Velocity profiles—plane passing through the middle of the semicircular gaps.

(a) the particle migration perpendicular to the flow direction;
(b) mass transfer between the phases;
(c) heat transfer between the phases;
(d) particle/particle interactions;
(e) flow boundary effects;
(f) particle shape effects.

In accordance with these simplifications, it is assumed that ash particle movement is governed only by momentum transfer between the phases. Momentum transfer between a single ash particle and the air stream is given by [13]

$$\frac{4\pi}{3}r_p^3\rho_p\frac{dv_p}{d\tau}=\frac{4\pi}{3}r_p^3\rho_p\phi(v-v_p)+\sum_{i=1}^{n}F_i - \frac{4\pi}{3}r_p^3\frac{\partial \mathbf{p}}{\partial r}+\frac{1}{2}\frac{4\pi}{3}r_p^3\rho\frac{D}{D\tau}(v-v_p) + Gr_p^2\sqrt{(\pi\rho\mu)}\int_0^{\tau}\frac{D}{D\tau}(v-v_p)\frac{d\tau}{\sqrt{(\tau_p-\tau)}}. \quad (1)$$

The terms on the right-hand side of equation (1) are the various forces acting on the particle in the air stream. The first term on the right-hand side is the drag force term, the second term the stream pressure

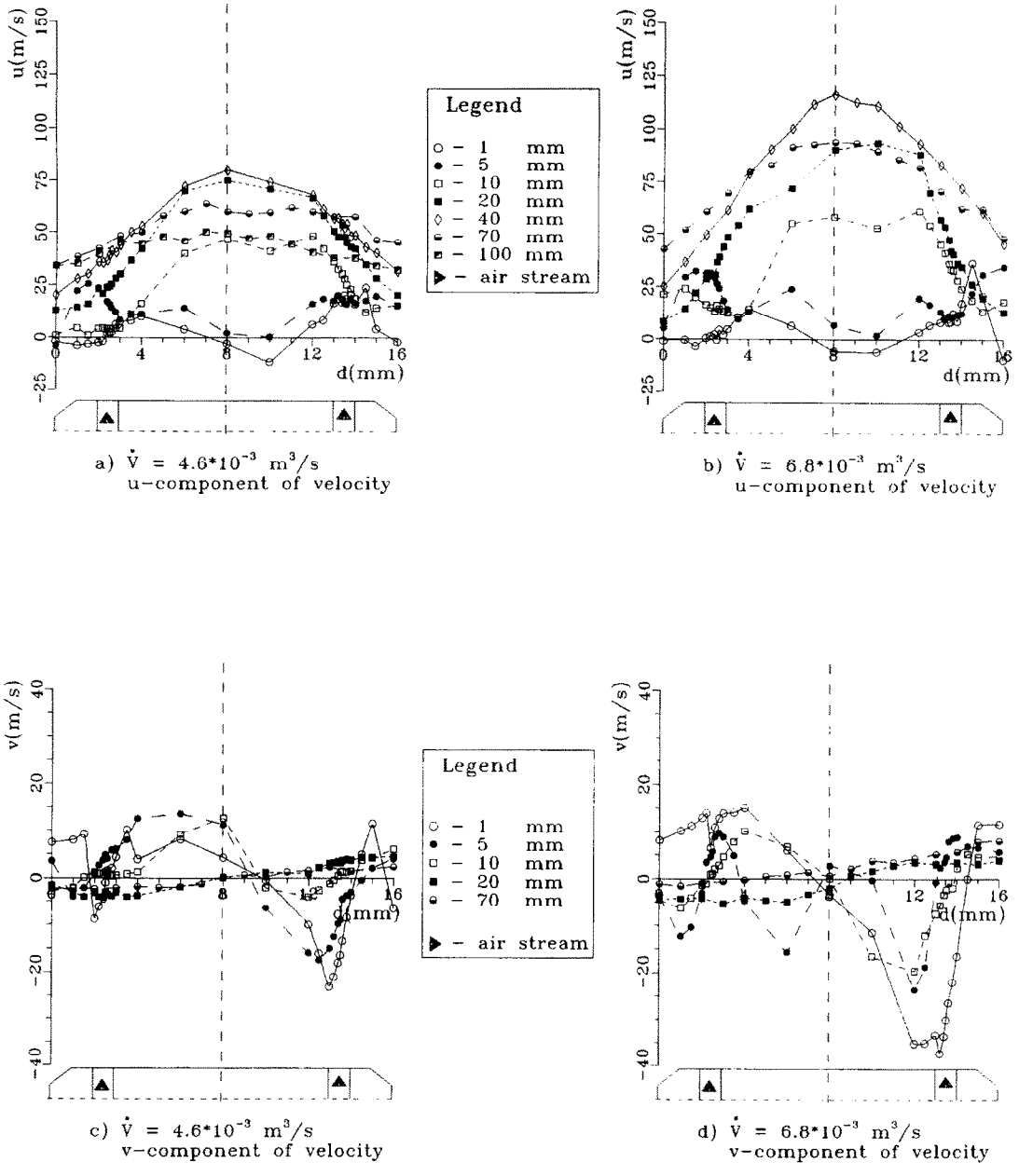

FIG. 4. Velocity profiles—plane passing through the connecting ribs.

gradient related forces, the third term the virtual mass related inertial forces, the fourth term the acceleration history related forces and the fifth term the external forces (gravity, electromagnetic forces).

The influence of pressure gradient related forces, virtual mass related inertial forces and forces due to the acceleration history is assumed considerably smaller than that of the drag force and external forces [14]. As the time constant, ϕ, is [13]

$$\phi = \tfrac{3}{8} C_D \frac{\rho}{\rho_p} \frac{|v-v_p|}{r_p} \tag{2}$$

equation (1) becomes

$$m_p \frac{dv_p}{d\tau} = \tfrac{1}{2}\rho C_D A_p (v-v_p)|v-v_p| + \sum_{i=1}^{n} F_i. \tag{3}$$

The drag coefficient, C_D, is given [10, 12] by

$$C_D = \frac{24}{Re_p}(1.0+0.15Re_p^{0.687}). \tag{4}$$

The Reynolds number is given [10] as

$$Re_p = \frac{\rho d_p |v-v_p|}{\mu}. \tag{5}$$

The particle characteristic time is [12]

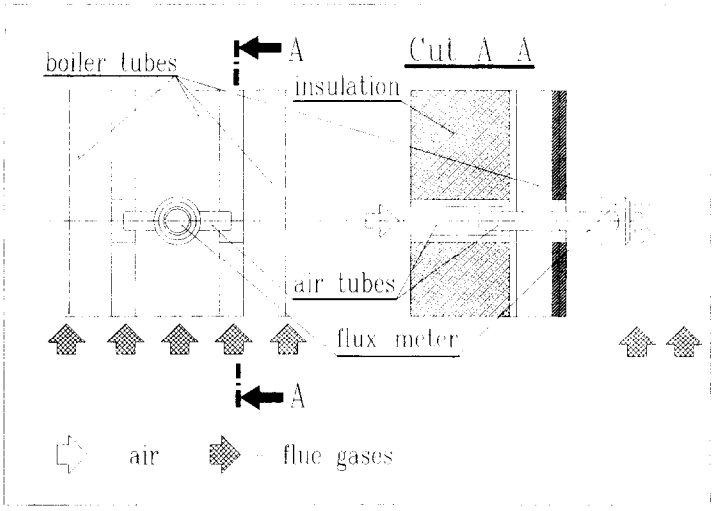

FIG. 5. Positioning of the 'clean' flux-meter.

$$\tau_p = \frac{m_p}{3\pi\mu f_p d_p}. \quad (6)$$

And f_p is equal [12] to

$$f_p = 1.0 + 0.15 Re_p^{0.687}. \quad (7)$$

According to equations (3)–(7), ash particle movement in the two-dimensional air flow, in the presence of gravity, is specified by a system of two scalar differential equations

$$\frac{du_p}{d\tau} = \frac{1}{\tau_p}(u - u_p) \quad (8)$$

$$\frac{dv_p}{d\tau} = \frac{1}{\tau_p}(v - v_p) - g\left(1 - \frac{\rho}{\rho_p}\right). \quad (9)$$

Computer code

The two-dimensional velocity field is computed in the pre-processor part of the computer code interpolating the experimental results obtained for the investigated air flows (4.6×10^{-3} and 6.8×10^{-3} m^3 s^{-1}). Particle trajectories are calculated using the Sharma method [14]. Assuming that the fluid velocity is constant during the short time interval, the analytic solution of equations (8) and (9) is [12]

$$u_p = u + (u - u_p^0)\, e^{(-\Delta\tau/\tau_p)} \quad (10)$$

$$v_p = v - (v - v_p^0)\, e^{(-\Delta\tau/\tau_p)} - g\tau_p[1 - e^{(-\Delta\tau/\tau_p)}]. \quad (11)$$

The particle position at the end of time interval $\Delta\tau$ is [12]

$$x = x_0 + (u_p - u_p^0)\frac{\Delta\tau}{2} \quad (12)$$

$$y = y_0 + (v_p - v_p^0)\frac{\Delta\tau}{2}. \quad (13)$$

The particle velocity at the moment of contact with the air stream is also calculated using equations (10) and (11), by assuming that the fluid velocity is equal to the furnace flue gas velocity.

Preliminary computation runs were used to define the optimal time steps that satisfy a step-size independent solution. The time intervals of $\Delta\tau' = 0.05\tau_p$ for the region external to the annulus gaps and $\Delta\tau'' = 0.001\Delta\tau'$ used in the computation satisfy the step independence condition.

The results of ash particle predictions

Ash particle trajectories were predicted for:

(a) particle diameter $D_p = 0.5$ mm;
(b) particle density $\rho_p = 1000$ kg m^{-3};
(c) flue gas velocity $V_{FG} = 8$ m s^{-1}.

These assumptions are also the limiting aerodynamic conditions encountered in power plant boiler furnaces. Predictions are made for the vertical particle–stream contact plane that is assumed the most disadvantageous (Fig. 5). This plane of contact coincides with the measuring plane normal to the connecting ribs. The experimental velocity data for this plane are used to calculate the velocity field in the pre-processor section of the computer code. Ash particle trajectories are computed for an air stream within a 10 mm radial distance from the centre of the receiving disc and at an axial distance of 1–40 mm from its surface. Computations are made at different incident contact angles and axial distances. The axial distances are varied in steps of 2 and 5 mm at axial distances of 1–10 and 10–40 mm, respectively. The incident angles are varied in 5° steps in the 0–80° range.

The predicted trajectories for both air flow rates and at several incident angles and axial distances are shown in Fig. 6. The streams of different symbols depict ash particle positions at subsequent points in time.

The simulation indicates that for an air flow rate of

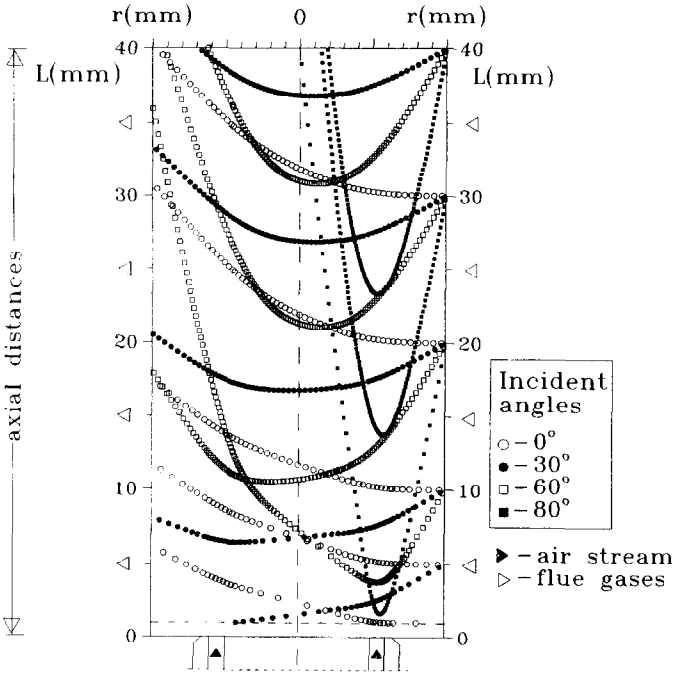

a) $\dot{V} = 4.6*10^{-3}$ m^3/s

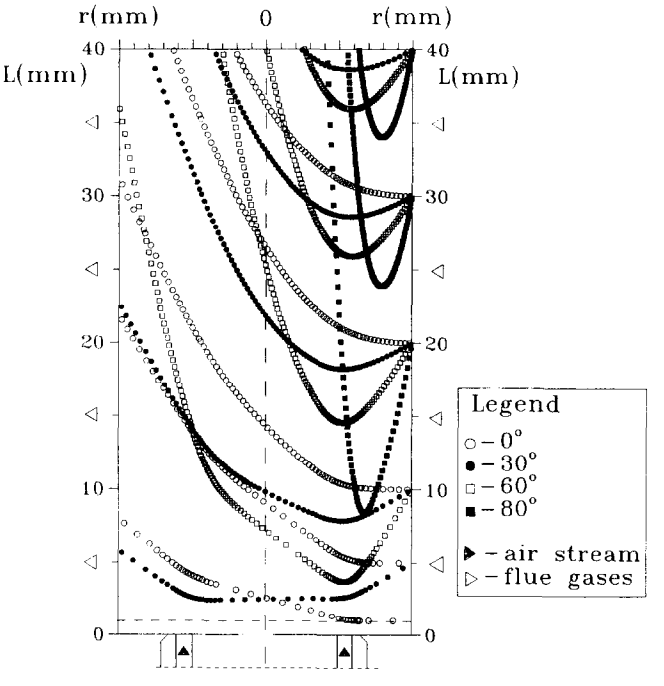

b) $\dot{V} = 6.8*10^{-3}$ m^3/s

FIG. 6. Ash particle trajectories.

6.8×10^{-3} m^3 s^{-1} the ash particles penetrate the air stream but none of them come into contact with the receiving disc. At a flow rate of 4.6×10^{-3} m^3 s^{-1}, contact between the receiving disc surface and the ash particles cannot be avoided for ash particles that enter the air stream at axial distances of 3–7 mm and at higher incident angles.

DISCUSSION

Experimental results

The measured downstream decrease of the u-component and changes in the shape of the velocity profile indicate the broadening of the air stream. According to our experimental results, this broadening starts near the flux-meter in the region at an axial distance of 1–5 mm from the flux-meter. The maximum measured u-component values monotonously decrease with increasing axial distance. The maximum measured u-component values at distances of 20 and 100 mm are 15 and 50% smaller, respectively, than the values measured at 1 mm from the flux-meter. The broadening of the air stream results in a gradual transformation from a toroidal to a conical shape. At an air flow rate of 6.8×10^{-3} m^3 s^{-1}, the air stream is fully conical at a distance of 20 mm from the flux-meter. At 4.6×10^{-3} m^3 s^{-1}, at the above distance the maximum values of the u-component are still measurable above the annular gaps. This indicates that the stream has not become totally conical. Results obtained at a distance of 40 mm show that the transformation is complete.

The measured negative values of the u-component indicate that recirculation occurs above the receiving disc and that an air vortex develops. Recirculation increases with an increase in the air flow rate. Our results indicate that the vortex exists in the centre of the air stream up to a distance of 5 mm at a flow rate of 4.6×10^{-3} m^3 s^{-1} and up to a distance of 10 mm at a flow rate of 6.8×10^{-3} m^3 s^{-1}.

Maximum values of the v-component occur 1 mm above the receiving disc. These values decrease with distance. Measured values were averaged over each full profile. These average values are depicted in Fig. 7. It is evident that in the vicinity of the receiving disc the average values decrease slowly with distance. A sudden decrease occurs at a distance of 10–40 mm. A 50% increase in the flow rate entails a 5–10% increase in the v-component average values.

Direction changes in the v-component direction at axial distances of 1–10 mm confirm the existence of an air vortex upon the receiving disc. The observed v-component direction indicates that near the flux-meter atmospheric air is sucked into the stream. This suction intensifies with the increase in the flow rate and is observed up to an axial distance of 5 mm.

Results obtained in the plane passing through the connecting ribs indicate that the ribs strongly affect the air stream in their vicinity. Considerably smaller

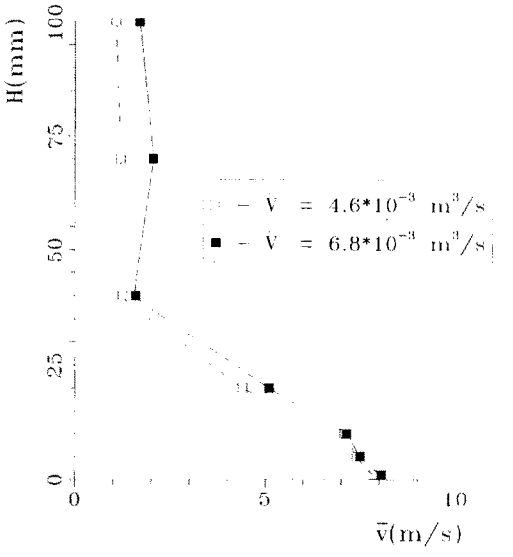

FIG. 7. Averaged values of the v-component of air velocity.

values of the u-component and greater values of the v-component are measured near the ribs. The effect is stronger at higher flow rates but it decreases downstream and at approximately the same distance at both flow rates (20 mm), it disappears completely.

The obtained experimental data were compared to analytically obtained velocity fields. The two-dimensional model for infinite gaps proposed by Rajaratnam [15], was used to obtain the latter. The principal assumptions incorporated into the model are that there is no interaction between the flow branches and that, according to dimensional analysis, the v-component of the air velocity can be neglected. These assumptions preclude the extraction of information on the v-component of the air velocity and the possible existence of air vortices. Only the comparison of u-component experimental data obtained in the plane perpendicular to the connecting ribs is possible.

The greatest discrepancy between experimental and analytical results is encountered in the potential core region (the region from the outlet to approximately 5 mm downstream). Measured values are 20% lower than analytically predicted for the 4.6×10^{-3} m^3 s^{-1} flow rate and 33% lower for the 6.8×10^{-3} m^3 s^{-1} flow rate. With an increase in distance, these differences decrease and at a distance of 20 mm, disappear completely. The analytically obtained values for the distance at which flow branch interaction commences are 22.5 mm at a flow rate of 4.6×10^{-3} m^3 s^{-1} and 21.0 mm at a flow rate of 6.8×10^{-3} m^3 s^{-1}. According to our experiments interaction is observed at a distance of 20 mm at 4.6×10^{-3} m^3 s^{-1} (15% nearer) and at a distance of 10 mm at 6.8×10^{-3} m^3 s^{-1} (50% nearer).

Our experimental set-up allows velocity measurements up to 350 m s^{-1} (75% greater than the maximum analytically obtained values). Thus, the

observed differences are due to scattering particle inertia and our neglecting the v-component of velocity. As a result of the design of the flux-meter with its sharp velocity increase at the gaps and the observed agglomeration, the seed particles cannot attain the fluid velocity instantaneously. In addition, the air vortex intensifies the broadening of the stream thus branches decreasing u-component values. The discrepancies observed in the potential core region are mostly due to scattering particle inertia and as a result of apparatus short comings. The discrepancies observed in the region adjacent to the potential core (up to 20 mm downstream) are mostly vortex effects and are due to analytical model simplifications.

Particle trajectories

In an attempt to predict ash particle trajectories we coupled an analytical model and experimentally obtained velocity field data with a view to observing the effect of the stream on the ash particle trajectories. Several simplifying assumptions are incorporated into the analytical model.

The first assumption is that particle migration perpendicular to the stream direction does not occur. Perpendicular particle migration is due to the radial pressure gradient in the stream and its influence on the particle movement is significant only if the flow is laminar. Experimental results indicate that the flow in the air stream is highly turbulent and the simplification mentioned is not detrimental to the analysis.

Mass transfer between phases is neglected. In tangentially fired boilers burning pulverized coal, all the devolatilization and combustion processes outside the furnace burner belt are over before ash particles reach the furnace walls. This simplification also has little effect on the analysis.

Due to the small dimensions ($d_p = 0.5$ mm) and lower temperatures (900–1200 K) the heat capacity of the particles is very small. It is assumed that at contact with the air stream, the ash particles instantaneously cool to the air stream temperature. Thus, the assumed absence of heat transfer between particles and air stream loses significance.

Due to stream/particle interaction, the particles alter flow conditions in their vicinity. If the volumetric concentration of the particles in the stream is high and the distances between them are small, the mentioned effects can superimpose creating local flow conditions different from those in the remainder of the stream. The limiting value at which particle/particle interaction occurs cited in the literature [12] is 1% volumetric concentration. In view of boiler furnace dimensions, fuel consumption, the fuel ash content, ash density and dimensions and the residence time of ash particles in the furnace, the volumetric concentration of the ash particles in the furnace is predicted at less than 0.05%. Accordingly, neglecting particle/particle interaction has no influence on the analysis.

The assumption that flow boundary effects can be neglected is due to the flow geometry. In the case under consideration, the furnace walls act as the only flow boundaries. As there is no direct contact between the air stream and the wall boundaries, this simplification does not affect the analysis.

According to the literature [16–18] ash particles can be assumed to be porous spheres. For the Reynolds numbers in question (N_{Re} are smaller than 1000) and intense turbulence there is no clear indication of the effect of surface roughness on particle trajectories [10].

Additional simplifications were introduced in solving equation (1). The pressure gradient, virtual mass and Basset term (second, third and fourth term on the right-hand side) of equation (1) are of the order of the gas/particle density ratio. For the incompressible air flow in our case this ratio is approximately 10^{-3} and the mentioned terms can be neglected. In our analysis we assume that, although the maximum measured values of the u-velocity component (140 m s^{-1} at an airflow rate of 6.8×10^{-3} m^3 s^{-1}) indicate that the flow is compressible and the air/particle density ratio grows, forces described by these terms can be neglected as compared to drag and gravitation. This simplification is made partly in view of the difference between experimental and in-plant operating temperature conditions. Velocity data were experimentally obtained for an air stream entering the environment at room temperature, and in actual operating conditions this temperature is expected to be in the 450–600°C range.

The velocity data used in the prediction of particle trajectories were experimentally obtained for up-ward flow opposite in direction to that of gravity while the predictions are made for flow perpendicular to the direction of gravity. It is assumed that the error due to the different flow geometries can be neglected due to the negligible mass of the scattering particles. Furthermore, the effect of the flue gas flow on the air stream velocity field is neglected because of the significant difference in the air and flue gas velocities in the region of interest.

Computer code input data are a function of the experimental data [17, 18]. Fractional analysis of the furnace ash particles indicates that the particles, the diameters of which are greater than 0.5 mm, make up far less than 1% of the total number of particles. The flue gas velocity in the furnace varies between 5 and 7 m s^{-1} and rarely exceeds 7.5 m s^{-1}. The density of the particles is reported to be in the 700–900 kg m^{-3} range.

The predicted trajectories indicate that, at 6.8×10^{-3} m^3 s^{-1} and for all the incident angles and positions of contact between the particles and air stream investigated, the impact of the ash particles on the receiving disc surfaces is prevented. At a flow rate of 4.6×10^{-3} m^3 s^{-1}, particle/receiving disc surface contact is possible only for particles entering the air stream at axial distances of 3–7 mm. As the ash particles cool as they penetrate the air stream, even in the case of contact, ash particle deposition is not to be expected. The initial trajectories of all the particles are

altered in such a manner that the particles hit furnace walls around the receiving disc or are carried downstream away from the flux-meter. The computation indicates a weak vortex trajectory effect. Due to the small negative u-component values in the vortex zone (maximum value measured is -11 m s^{-1}) and the short residence time (particles reside in the vortex zone for less than 2 ms), particle inertia prevails over the vortex drag force and the stream carries them away. Because of the air stream, ash particles reside in the zone above the receiving disc 50–100% longer than they would if there was no protective air stream. Due to the low initial concentration of ash particles, the increase of concentration due to the longer residence time does not significantly affect radiative heat transfer between the flame and the 'clean' heat flux-meter.

CONCLUSIONS

According to the experimentally obtained velocity data and trajectory simulations, the air stream successfully prevents ash deposit formation. The influence of the connecting ribs on the air stream diminishes downstream. If the flux-meter is correctly positioned on the boiler tube (Fig. 5), the connecting rib caused flow instabilities have no effect on the protection against ash deposit formation. The influence of the air vortex formed in the centre of the toroidal zone of the stream on ash particle trajectories is insignificant and does not affect the protective function. The conical transformation of the air stream together with the low initial ash particle volume concentration prevents a significant increase in the particle concentration above the receiving disc.

REFERENCES

1. D. Savic, N. Afgan, Lj. Jovanovic, S. Markovic, P. Pavlovic and B. Arsic, Investigation of tendencies of the lignite from Kolubara, Kostolac and Kosovo basins towards the formation of deposits on heat transfer surfaces during combustion in a boiler furnace, *Bull. Serbian Acad. Sci.* **65**(15), 14–79 (1974).
2. D. Savic, N. Afgan, V. Jovic, Lj. Jovanovic, S. Markovic and P. Pavlovic, Effect of ash deposits on heat transfer performance in pulverized lignite fired boilers. In *Future Energy Production*. Hemisphere, New York (1976).
3. W. Clay and I. S. Davidson, Heat flux-meters in furnace boilers to monitor slag deposition, *Proc. IMECO Symp. on Thermal and Temperature Measurements in Science and Industry*, Liverpool, pp. 345–375 (1987).
4. A. K. Chambers, J. R. Wynnyckyj and E. H. Rhodes, Development of a monitoring system for ash deposits on boiler tube surfaces, *Can. J. Chem. Engng* **59**, 230–235 (1981).
5. A. K. Chambers, J. R. Wynnyckyj and E. H. Rhodes, A furnace wall ash monitoring system for coal fired boilers, *Trans. ASME, J. Engng Pwr* **103**, 532–537 (1981).
6. E. W. Northower, The CERL Dometer—a radiant heat flux in tube metal temperature system for highly rated boilers, *CEGB Disclosure Bull.* No. 294 (1978).
7. S. B. H. C. Neal, E. W. Northower and J. A. Hitchcock, Some new devices for the measurement of heat flux in power station boiler furnaces, *J. Inst. Energy* **3**, 8–14 (1982).
8. M. Matovic, C. Tropea and R. Martinuzzi, Frequency estimation of LDA signals by model parameter estimation, *Proc. Int. Meeting on the Use of Computer in LDA Measurements*, ISL, Saint Louis, France (1988).
9. M. Matovic and C. Tropea, Estimation of LDA signal frequency using the auto variance lag ratio method, *J. Phys. E.: Sci. Intrum.* **22**, 631–637 (1989).
10. E. Clift and W. H. Gavin, Motion of entrained particles in gas streams, *Can. J. Chem. Engng* **49**, 439–448 (1971).
11. F. Durst, D. Milojevic and B. Schonug, Eulerian and Lagrangian predictions of particulate two-phase flows—a numerical study, *Appl. Math. Modelling* **8**, 101–115 (1984).
12. D. Z. Milojevic, Two dimensional turbulent flow of fluid particle mixtures (in Serbo-Croatian), Ph.D. Thesis, Belgrade University, Belgrade (1986).
13. S. Sou, *Gidrodinamika monofaznih sistem*, p. 47. Mir, Moskva (1971).
14. C. T. Crowe, M. P. Sharma and D. E. Stock, The particle-source-in cell (PSI CELL) model for gas droplet flows, *Trans. ASME, J. Fluids Engng* 325–332 (June 1977).
15. N. Rajaratnam, *Turbulent Jets*, Developments in Water Science No. 5. Elsevier, Amsterdam (1976).
16. E. Raask, Cenospheres in pulverized fuel ash, *J. Inst. Fuel* 339–344 (1968).
17. Lj. L. Jovanovic, *Boiler Surface Fouling and Cleaning* (in Serbo-Croatian), pp. 57–71. IBK-Vinca, Belgrade (1980).
18. B. Repic, B. Arsic and Lj. L. Jovanovic, Fouling of the furnace surfaces of VU-40 industrial boilers (in Serbo-Croatian), IBK-ITE 704, Boris Kidric Institute, Belgrade (1988).

UN FLUXMETRE THERMIQUE POUR DES SYSTEMES AVEC DEPOT DE CENDRE—I. PREVENTION DU DEPOT

Résumé—On a développé un fluxmètre thermique "propre" refroidi par l'air. Les résultats sont présentés pour l'étude expérimentale et théorique du rideau d'air refroidissant qui protège aussi la formation du dépôt de partiqules. Les champs de vitesse pour deux débits et dans deux plans perpendiculaires d'écoulement sont précisés. Ces données sont utilisées pour calculer les trajectoires des particules de cendre. Ces trajectoires montrent que l'efficacité de l'écoulement d'air protège l'élément récapteur du fluxmètre "propre" contre la formation d'un dépôt de cendre.

EIN WÄRMEFLUSSMESSGERÄT FÜR SYSTEME ZUR ÜBERWACHUNG DER ASCHEABLAGERUNG—I. VERHINDERUNG DER ASCHEABLAGERUNG

Zusammenfassung—Es wurde ein luftgekühltes "sauberes" Wärmestromdichtemeßgerät entwickelt. In der vorliegenden Arbeit werden die Ergebnisse einer experimentellen und analytischen Untersuchung des kühlenden Luftvorhangs vorgestellt, der zusätzlich auch der Ascheablagerung entgegenwirkt. Unter Verwendung eines LDA werden die Geschwindigkeitsfelder bei zwei unterschiedlich großen Luftströmen und bei zwei unterschiedlichen Strömungsrichtungen bestimmt. Mit Hilfe dieser Daten werden die Trajektoren von Aschepartikeln berechnet. Diese zeigen, daß der Luftstrom die Umgebung des "sauberen" Wärmestromdichtemeßgeräts vor einer Ascheablagerung wirksam schützt.

ИЗМЕРИТЕЛЬ ТЕПЛОВОГО ПОТОКА В СИСТЕМАХ КОНТРОЛЯ ОТЛОЖЕНИЙ ЗОЛЫ—I. ПРЕДОТВРАЩЕНИЕ ОТЛОЖЕНИЙ ЗОЛЫ

Аннотация—Разработан измеритель "чистого" теплового потока, охлаждчемый воздушным потоком. Представлены результаты экспериментального и аналитического исследований завесы охлаждающего воздушного потока, которая также предотвращает образование отложений частиц. С использованием лазер-допплеровского анемометра получена карта полей скоростей при двух различных скоростях воздушного потока в двух перфендикулярных плоскостях. На основе этих данных рассчитываются траектории частиц золы. Рассчитанные траектории свидетельствуют о том, что воздушный поток эффективно предохраняет воспринимающий элемент измерителя от отложения золы.